https://doi.org/10.5194/wes-2022-91
Preprint. Discussion started: 10 October 2022

eawe european academy of wind energy
Open Access WIND ENERGY SCIENCE DISCUSSIONS

Aeroelastic Validation of the Offshore Wind Energy Simulator for Vertical-Axis Wind Turbines

Kevin R. Moore[1] and Brandon L. Ennis[1]

[1]Sandia National Laboratories *, PO Box 5800 MS 0717 Albuquerque, NM 87185

Correspondence: Kevin R. Moore (kevmoor@sandia.gov)

Abstract.

Vertical-axis wind turbines (VAWTs) offer some unique advantages over traditional designs, particularly for floating offshore and certain distributed wind applications. However, the modeling capabilities that exist for VAWT designs greatly lags those for the traditional horizontal-axis wind turbines (HAWTs). Differences between vertical and horizontal turbines necessitates several key additions in modeling, including the aerodynamic model, as well as solving a fundamentally different structural mesh. The Offshore Wind ENergy Simulator (OWENS) is specifically formulated to fulfill these requirements. This paper presents validation cases of this tool for modal, centrifugal, gravitational, startup, normal operation, and shutdown analyses. The aeroelastic validation is performed with increasing complexity from analytical test cases to an experimental VAWT. Validation data are taken from the Sandia National Laboratories 34 meter research turbine. The results of the validation cases are presented and examined.

1 Introduction

Vertical-axis wind turbines (VAWTs) have been the subject of research and development for nearly a century (Darrieus, 1926). However, this turbine architecture has fallen in and out of favor on multiple occasions. Beginning in the late 1970s, the U.S. Department of Energy sponsored an extensive experimental program through Sandia National Laboratories which produced a mass of experimental data from several highly instrumented turbines. Turbines designed, built, and tested include the 2 meter, 5 meter, 17 meter, and 34 meter and their respective configurations (Blackwell et al., 1976), (Sheldahl et al., 1980), (Worstell, 1981), (Ashwill, 1992) .This program kicked off a commercial collaboration and resulted in the FloWind turbines (Alcoa, 1983). The FloWind turbines had several notable design changes from the experimental turbines that, in conjunction with a general lack of understanding regarding predicting fatigue at the time (Packman, 1988), led to the majority of the turbines failing prematurely during the late 80s.

More recently, beginning in the 2010s, interest has resurged for VAWTs for certain applications. Differing cost relationships for floating offshore wind energy and distributed wind systems relative to land-based utility wind systems can favor VAWT

*Sandia National Laboratories is a multimission laboratory managed and operated by National Technology and Engineering Solutions of Sandia, LLC., a wholly owned subsidiary of Honeywell International, Inc., for the U.S. Department of Energy's National Nuclear Security Administration under contract DE-NA-0003525

https://doi.org/10.5194/wes-2022-91
Preprint. Discussion started: 10 October 2022

designs, due to reductions in support structure and maintenance costs. The vertical turbine's lower center of gravity, easy access to the drivetrain, and removal of active components (yaw and, in some cases, pitch systems) offer significant advantages for these concepts. However, the ability to accurately model and design these complex, flexible systems is critical to assess their performance and enable commercial success.

Specifically, this paper will review the aeroelastic code, present the experimental validation data, and show simulation comparisons against a series of analytical cases and several experimental tests from the Sandia 34 meter turbine. The validation cases consist of multiple levels of cantilever beam analyses in addition to full turbine analyses, including modal, parked gravity loading, still air forced centrifugal loading, normal operation, and emergency shutdown.

2 OWENS (Offshore Wind ENergy Simulator)

The Offshore Wind ENergy Simulator (OWENS) was originally developed to meet the needs for design and simulation of VAWTs. The structural module solves the equations of motion for a gyric system in the rotating hub frame for ease of inclusion of centrifugal effects (Meirovitch, 1980). A finite element mesh is used to represent the rotor and elasticity and is solved through the use of Timoshenko beam elements (Owens, 2013). Beyond the standard Timoshenko finite element formulation, OWENS includes VAWT-related considerations including gyroscopic, spin softening, centrifugal stiffening, and Coriolis effects. The structural model has been previously validated for modal resonant predictions, and had notable verification comparisons between the different modes of unsteady operation (Owens, 2013). This code has been rewritten in the Julia programming language (Bezanson et al., 2017) and formulated to enable two-way coupled dynamic simulations necessary for design and optimization of floating vertical-axis wind turbines. The improved capabilities for OWENS includes; 1) Aerodynamic simulation using the Actuator Cylinder or Double Multiple Streamtube models in either one-way and two-way coupling with modeling and numerical improvements for simulating curved blades (Moore and Ennis, 2022), 2) Translation into the Julia programming language, enabling significant speedup, automatic differentiation, and the ability to ship compiled binaries or shared libraries without extensive code modifications, 3) All of the necessary preprocessing including mesh generation, sectional property calculation, and data reformatting are now within a single automated module as opposed to multiple manual file-based operations, 4) The major components of the code have been modularized and are drive by a glue code which enable easy integration of alternate models. The major modules are as follows:

- OWENS: combines the modules into a continuous analysis workflow from basic parametric inputs to response outputs for steady, unsteady, and modal analyses. While it has been tuned for stability and accuracy, it also makes a wide range of fidelity and solution parameters/flags accessible to the user to enable use-case-specific tuning for accuracy and stability. This also includes the ability to modify control inputs for the full range of typical control elements.

- VAWTAero: consists of steady and unsteady analysis methods for 3D VAWTs (Double Multiple Streamtube and Actuator Cylinder), including dynamic stall models, multiple Reynolds/Mach/Family of airfoils lookup, and a new unsteady method (RPI) which enables faster than real-time calculations for aerodynamic only calculations of full turbines. Ad-

https://doi.org/10.5194/wes-2022-91
Preprint. Discussion started: 10 October 2022

eawe european academy of wind energy
Open Access WIND ENERGY SCIENCE DISCUSSIONS

ditionally, the aerodynamic models were reformulated to properly account for curved blades which resolves a major source of error for Darrius configurations. The OpenFAST (NREL, 2022) InflowWind library is optionally coupled to VAWTAero for turbulent inflow simulations.

- GyricFEA: is a gyric beam finite element model built on Timoshenko elements. It consists of linear and nonlinear unsteady analysis, modal analysis with centrifugal stiffening, reduced order model analysis (using mode shapes), and steady state analysis. It verifies well against geometrically exact beam theory even for moderate (20% of length) deflections.
- ModelGen: takes in general geometric and sectional composite layup inputs and generates a custom mesh and calculates sectional properties via NREL's PreComp (Bir, 2006) code (translated to Julia as well). While it does have the ability to output a full range of input files, it is designed for efficient direct coupling to the finite element solver.
- Simplified coupling to external modules for pre and post processing such as rainflow counting, classical lamination theory and failure, and simplified analytical buckling theory, in addition to geometrically exact beam theory for the structural solver.
- Additionally, direct coupling to the OpenFAST Hydrodyn and Moordyn modules have been done to enable floating platform simulations, which will be covered in a separate publication.

3 Verification and Validation

To verify and validate the OWENS code, we take a sequential approach which increases in complexity as is typically prescribed for a validation hierarchy (Oberkamph et al., 2003). Since the base elastic solution of the structural code was not previously verified, we start with several simple analytical cases and use a geometrically exact beam theory code for code-to-code comparison (Yu and Blair, 2012). These comparisons include cantilever and centrifugal deflection, modal analysis, and Campbell Diagram analysis in addition to unsteady harmonic forcing. We then transition to the Sandia 34m turbine and conduct verification and validation relating to sectional properties, modal analysis, steady state gravitational and centrifugal loading, and a variety of unsteady 2-way aeroelastic performance cases.

https://doi.org/10.5194/wes-2022-91
Preprint. Discussion started: 10 October 2022

eawe european academy of wind energy
Open Access WIND ENERGY SCIENCE DISCUSSIONS

3.1 Structural Solver Validation

To validate the structural dynamics portion of the code, we begin by using a simple cantilever beam to verify modal predictions including centrifugal effects, steady state tip displacement, steady state centrifugal loads displacement, and dynamic response. The beam used is a simple rectangular cross section with fixed-free boundary conditions and no gravity loads. Table 1 gives the parameters used while Table 2 and Table 3 give the sectional stiffness and mass matrices which are used for each element along the span.

Table 1. Simple cantilever beam definition.

Name	Value
length (L)	0.5 m
width (b)	0.05 m
height (h)	0.02 m
area (A)	$b * h$
elastic modulus (E)	210 GPa
poisson ratio (v)	0.28
shear modulus (G)	$\frac{E}{2(1+v)}$
density (ρ)	7800 kg/m^3
moment of inertia (I_{yy})	$b * h^3/12$ m^4
moment of inertia (I_{zz})	$b^3 * h/12$ m^4
torsional moment of inertia (J)	I_{yy}+I_{zz} m^4
tip load (P)	0:1e4:1e5 N
RPM	0:1e4:1e5 RPM
number of elements	40

Table 2. Simple cantilever beam sectional stiffness matrix.

$E * A$	0	0	0	0	0
0	$G * A$	0	0	0	0
0	0	$G * A$	0	0	0
0	0	0	$G * J$	0	0
0	0	0	0	$E * I_{yy}$	0
0	0	0	0	0	$E * I_{zz}$

Table 3. Simple cantilever beam sectional mass matrix.

$\rho * A$	0	0	0	0	0
0	$\rho * A$	0	0	0	0
0	0	$\rho * A$	0	0	0
0	0	0	$\rho * J$	0	0
0	0	0	0	$\rho * I_{yy}$	0
0	0	0	0	0	$\rho * I_{zz}$

https://doi.org/10.5194/wes-2022-91
Preprint. Discussion started: 10 October 2022

eawe european academy of wind energy
Open Access WIND ENERGY SCIENCE DISCUSSIONS

3.1.1 Modal Analysis

The analytical expression for the natural frequencies (ω_n in rad/s) of a cantilever beam is shown in Eq. (1). The analytical correction factor k_n as described in (Inman, 2014) is 1.875 for the first mode, 4.694 for the second, and 7.855 for the third.

$$\omega_n = \sqrt{\frac{E * I_{yy}}{\rho * A}} * \left(\frac{k_n}{L}\right)^2 \tag{1}$$

Table 4 gives the resulting modal frequencies and relative error. Note that while not shown, the mode shapes also match well. We also introduce the previously verified an validated geometrically exact beam theory (Yu and Blair, 2012) (Wang et al., 2013) (Hodges, 2006) via GXBeam.jl (McDonnell and Ning, 2022), which we use for code-to-code comparison in later analyses as needed in addition to using it as an optional alternative to the Timoshenko beam elements within the OWENS dynamic simulations. We include comparisons here against the analytical test cases to build confidence for the more complex analyses which do not have analytical solutions.

Table 4. Simple cantilever beam modal results.

Mode	Analytical (Hz)	OWENS (Hz)	OWENS Error (%)	GXBeam (Hz)	GXBeam Error (%)
1	67.05	66.98	0.11	66.99	0.09
2	420.21	417.17	0.72	418.02	0.52
3	1176.72	1157.48	1.63	1163.03	1.14

3.1.2 Tip Deflection with Tip Point Load

We now use the same beam but look at the tip deflection from a constant tip load. The analytical expression (James M. Gere, 2013) is shown in Eq. (2). Table 5 gives the resulting tip deflection and relative error; we again include GXBeam results to build confidence. Note that the analytical expression is linear while OWENS and GXBeam are able to run in both linear and nonlinear modes.

$$\delta_i = \frac{P_i L^3}{3 E I_{yy}} \tag{2}$$

Table 5. Simple cantilever beam linear tip deflection for three sample load results.

Load (N)	Analytical (m)	OWENS (m)	OWENS Error (%)	GXBeam (m)	GXBeam Error (%)
1E4	0.0595	0.0595	0.045	0.0593	0.101
5E4	0.298	0.297	0.045	0.298	0.101
1E5	0.595	0.595	0.045	0.596	0.101

https://doi.org/10.5194/wes-2022-91
Preprint. Discussion started: 10 October 2022

eawe european academy of wind energy
Open Access WIND ENERGY SCIENCE DISCUSSIONS

Figure 1 gives a visual representation of both nonlinear and linear beam shapes under load. Since the deflection is greater than 20% of the beam length, the fundamental assumptions of the Timoshenko formulation begin to be violated and the solutions begin to differ. For this case, there is a 3.26% difference in the nonlinear tip deflection. Also note that OWENS is formulated to use only follower forces, which are forces applied that maintain the orientation relative to the beam regardless of the beam's deflected state. Follower forces were used in GXbeam for consistency between the two models.

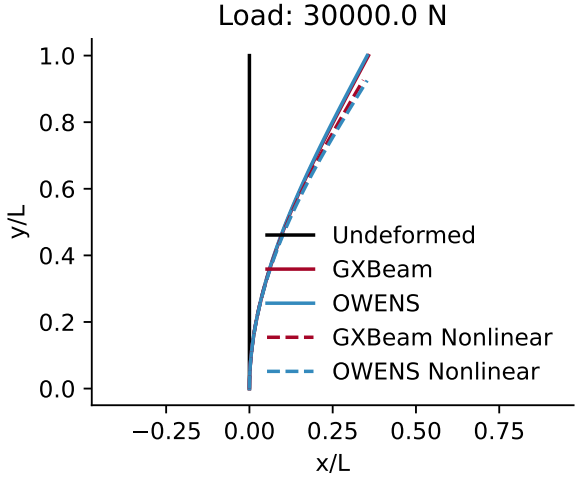

Figure 1. Straight beam deformed mesh for both linear and nonlinear analysis up to 30% tip deflection compared to length.

3.1.3 Centrifugal Force Deflection

Modeling a spinning beam with a bend exercises the ability to predict centrifugal effects on multiple structural degrees of freedom. The beam tested is the same as the previous examples, but with a 45 degree bend in the middle. Figure 2a shows the beam shape and an example deflection for relatively high RPM for both linear and nonlinear analysis. Rotation is about the z-axis or out of the page around the fixed end. This case, in addition to the tip deflection at varying RPM (Fig. 2b), shows excellent agreement between the two codes.

https://doi.org/10.5194/wes-2022-91
Preprint. Discussion started: 10 October 2022

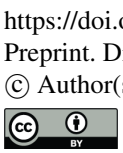

eawe european academy of wind energy
Open Access WIND ENERGY SCIENCE DISCUSSIONS

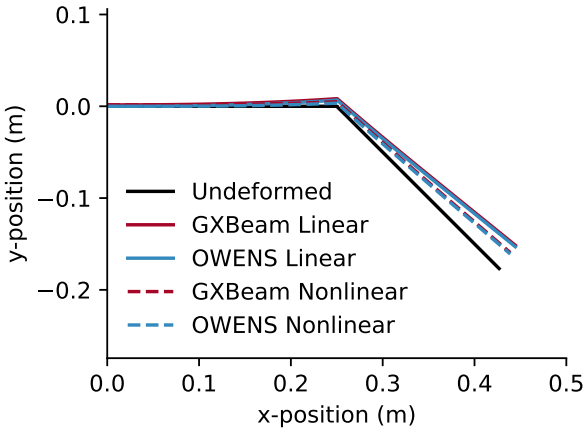

(a) Example geometry and deflection at 6000 RPM with excellent agreement.

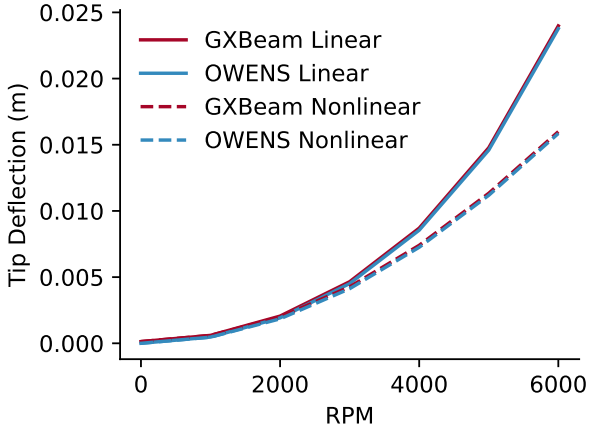

(b) Tip deflection for varying RPM levels with excellent agreement.

Figure 2. Bent cantilever beam deflection undergoing rotation about the z axis (out of the page).

3.1.4 Modal Analysis with Centrifugal Stiffening

A spinning beam which undergoes significant deformation experiences centrifugal stiffening which in turn affects the natural frequencies. Accurate prediction of this phenomenon is important for large wind turbines as the rotating modal frequencies can overlap with the blade pass forcing frequencies in operation. Figure 3 shows the resulting Campbell diagram of the spinning beam with a bend and reveals excellent agreement between the two codes for the lower frequencies, and a maximum 2.8% error for the 6th mode, a relatively complex coupled bend-twist torsional mode with three neutral points.

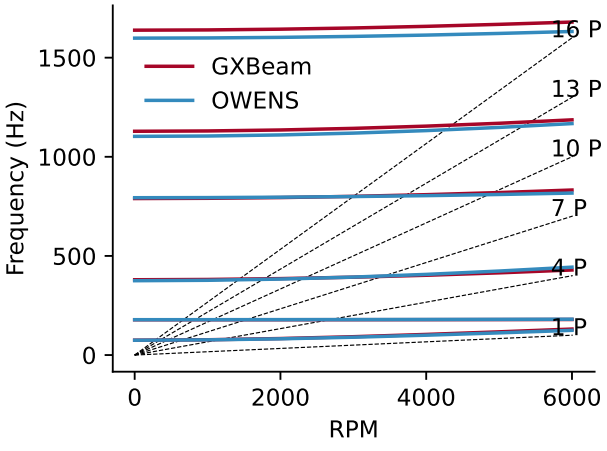

Figure 3. Campbell diagram analysis of the bent cantilever beam undergoing rotation about the z (out of the page) axis.

https://doi.org/10.5194/wes-2022-91
Preprint. Discussion started: 10 October 2022

eawe european academy of wind energy
Open Access WIND ENERGY SCIENCE DISCUSSIONS

3.1.5 Unsteady Tip Forcing

The test cases so far have been for static or steady state analyses. To test the dynamic response, we switch beam properties to enable more apparent harmonic frequency excitement. For this test, we use a straight beam with 20 elements, the properties given in Eqs. (3) and (4), and apply a sinusoidal forcing to the tip of -1e5*sin(20*t) ((Wang et al., 2013)). Additionally, damping coefficients of 0.005 were applied to both OWENS and GXBeam. This value was chosen to allow for resonance without allowing the high frequency content to dominate the solution. We should note that there is some difference in how the structural damping coefficients are applied between the two codes due to their different solution methodologies, which in turn causes some discrepancies in the solution, but still allows for a meaningful qualitative comparison. GXBeam applies the damping coefficients directly to the strains while OWENS applies them to the internal damping matrix.

$$\text{Mass Matrix} = \begin{bmatrix} 258.035 & 0.0 & 0.0 & 0.0 & 0.0 & 0.0 \\ 0.0 & 258.035 & 0.0 & 0.0 & 0.0 & 0.0 \\ 0.0 & 0.0 & 258.035 & 0.0 & 0.0 & 0.0 \\ 0.0 & 0.0 & 0.0 & 48.59 & 0.0 & 0.0 \\ 0.0 & 0.0 & 0.0 & 0.0 & 2.172 & 0.0 \\ 0.0 & 0.0 & 0.0 & 0.0 & 0.0 & 46.418 \end{bmatrix} \tag{3}$$

$$\text{Stiffness Matrix} = \begin{bmatrix} 2.389E+09 & 0.0 & 0.0 & 0.0 & 0.0 & 0.0 \\ 0.0 & 4.334E+08 & 0.0 & 0.0 & 0.0 & 0.0 \\ 0.0 & 0.0 & 2.743E+07 & 0.0 & 0.0 & 0.0 \\ 0.0 & 0.0 & 0.0 & 2.167E+07 & 0.0 & 0.0 \\ 0.0 & 0.0 & 0.0 & 0.0 & 1.970E+07 & 0.0 \\ 0.0 & 0.0 & 0.0 & 0.0 & 0.0 & 4.406E+08 \end{bmatrix} \tag{4}$$

The resulting base loads are shown in Figs. 4 to 6. The damped natural frequency of the solution matches and despite the difference in damping formulation, the root mean square values vary by 32%, 16%, and 9% for the three comparison loads. If the GXBeam damping gains are tuned, the error can be decreased to below 5% for all cases, but defining a relationship between the structural damping methods is not necessary for this qualitative verification case. Increasing the damping coefficients produces a similar level of agreement between the two models, but with attenuated amplitude and frequency as expected.

https://doi.org/10.5194/wes-2022-91
Preprint. Discussion started: 10 October 2022

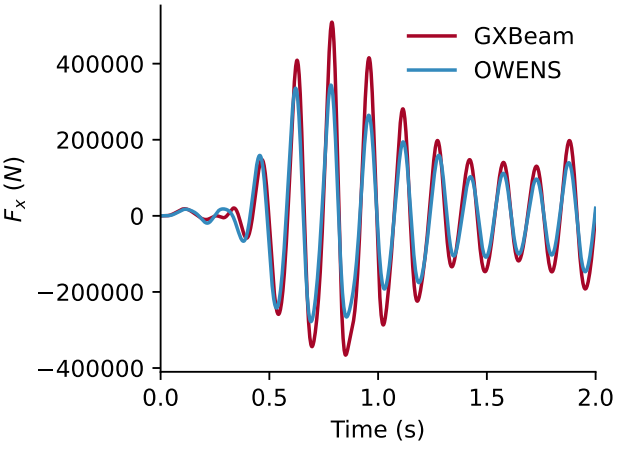

Figure 4. X-direction reaction force at the beam root.

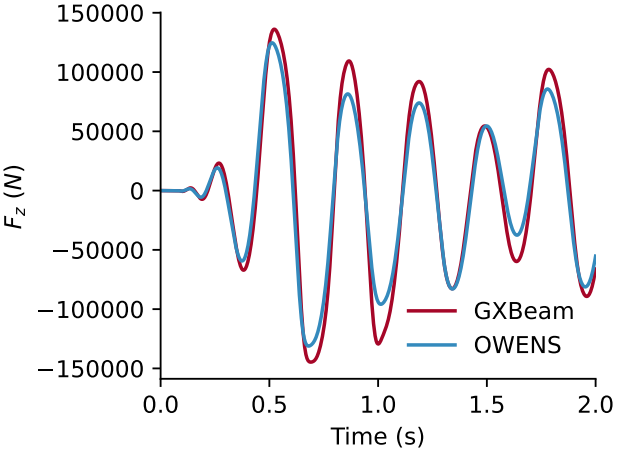

Figure 5. Z-direction reaction force at the beam root.

https://doi.org/10.5194/wes-2022-91
Preprint. Discussion started: 10 October 2022

eawe european academy of wind energy
Open Access WIND ENERGY SCIENCE DISCUSSIONS

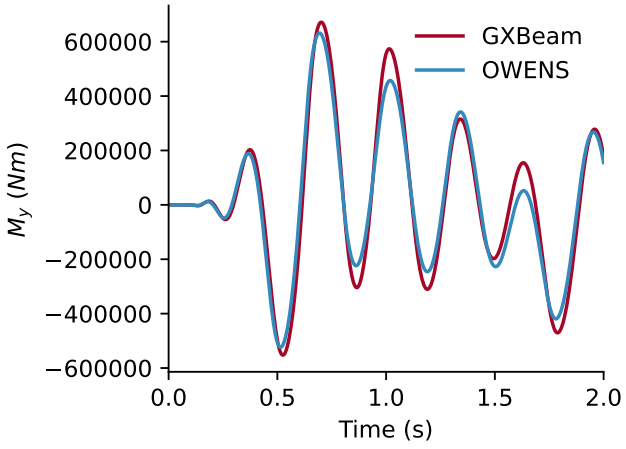

Figure 6. Reaction moment about the Y-axis at the beam root.

3.2 SNL 34m Structural Validation

Vertical-axis turbine experimental campaigns at Sandia National Laboratories extended over a period of nearly two decades, culminating with the design and testing of a highly instrumented 34 meter diameter VAWT (see Fig. 7). More specific details than are given here are contained in (Ashwill, 1992). In summary, this turbine had two blades, rigid blade mounts, and top-mounted guy wires for support. The blades were comprised of three unique blade sections as depicted in Fig. 8b, and made of 6065-T6 aluminum. The overall geometric dimensions of each blade section, its chord, and respective airfoil section can be seen in Fig. 8a.

https://doi.org/10.5194/wes-2022-91
Preprint. Discussion started: 10 October 2022

Figure 7. Sandia 34 meter VAWT in Bushland, Texas. Photo used with permission from Sandia National Laboratories.

There were distributed strain gauges along the turbine blades which were used to measure the blade response to parked gravitational loads, forced centrifugal loads, and a variety of unsteady operational loads. The majority of the time-domain data that were preserved in technical reports focuses on the upper and lower root sections of the turbine, where the loads tend to be the highest. The remaining data were recorded in statistical values as will be discussed in later sections.

The Sandia 34m turbine blades were constructed in three sections as shown in Fig. 8. As the most fundamental starting point to validate the SNL 34m structural response, we compare the experimental sectional properties (Sutherland, 1988) to the calculated properties in Table 6. Calculated properties are computed from from PreComp (Bir, 2006), approximating the aluminum skin and shear webs as lamina to comply with the expected composite layup inputs. The tower was comprised of a simple aluminum tube 3 meters in diameter and 12.5 mm thick.

Table 6. Comparison of Blade Sectional Properties.

Section	EA			EI Flap			EI Lag		
	Exp.	OWENS	Error (%)	Exp.	OWENS	Error (%)	Exp.	OWENS	Error (%)
Outer	2.632e9	2.599e9	1.25	1.649e7	1.674e7	1.52	2.744e8	2.841e8	3.53
Mid	1.478e9	1.498e9	1.38	5.197e6	5.267e6	1.36	1.125e8	1.130e8	0.42
Inner	1.185e9	1.201e9	1.32	3.153e6	3.195e6	1.32	6.674e7	6.762e8	1.32

https://doi.org/10.5194/wes-2022-91
Preprint. Discussion started: 10 October 2022

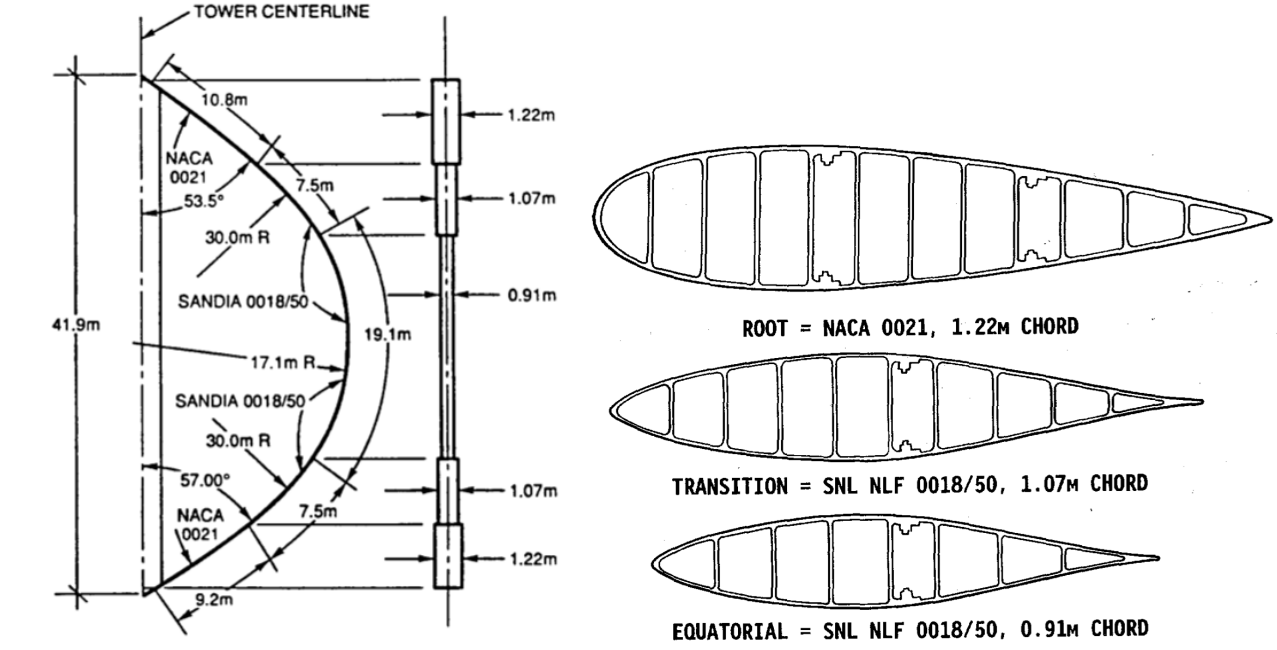

(a) Turbine Geometry.

(b) Sectional Geometry.

Figure 8. Sandia 34 meter shape definitions. Images to scale.

3.2.1 Campbell Diagram for the 34m

Using the blade and tower properties, we construct an accompanying OWENS mesh and run modal analyses with successively increasing RPM to create a Campbell diagram. The mesh is comprised of independent tower, blades, and the root fasteners, which were modeled as shallow struts. The root fasteners have the same properties as the blade base sections. These sections are combined via rigid joints to create the rotating structure. OWENS solves in the rotor frame of reference, and so the bottom node is fixed in all degrees of freedom and the top is fixed in planar and vertical translation to represent the effect of the upper guy wire supports on the test turbine. Figure 9 shows the response of both GXBeam and OWENS against the experimental data. The experimental turbine did not have a truly fixed top but was rather constrained by guy cables. The first tower mode in the presence of the cable pretension and stiffness is identified in Fig. 9 and would be captured if elements were added to the mesh that approximated the spring-like nature of the cables. However, the predicted blade modes do not differ appreciably.

https://doi.org/10.5194/wes-2022-91
Preprint. Discussion started: 10 October 2022

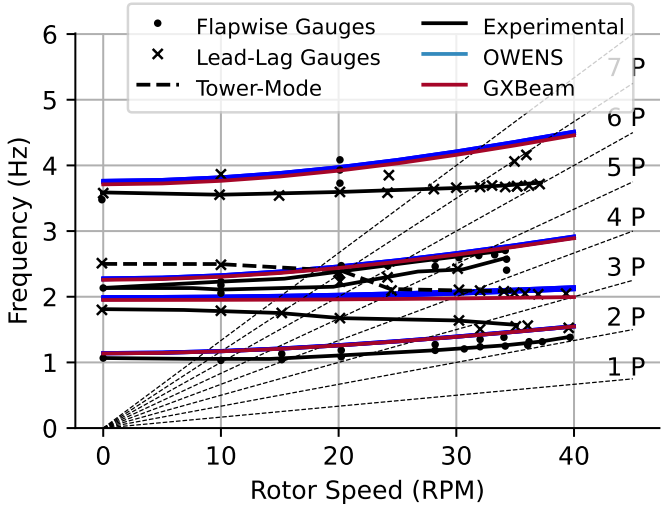

Figure 9. Campbell diagram of the 34 meter turbine showing strain gauge measurements, OWENS, and GXBeam predicted frequencies.

3.2.2 Static Gravity Loads

During construction of the turbine, the blade instrumentation was zeroed in a relaxed ground state prior to mounting the blades. Once the blades were mounted, the strain was recorded, which captures the gravity loads. In the original source, a simplified stress was reported, which was the measured surface strain multiplied by the material modulus of elasticity. Figure 10 shows the experimental and predicted gravity loads showing good agreement in magnitude and form with some under-prediction at the 35 meter span position. The original report (Sutherland, 1988) included predicted loads from finite element analysis which also under-predicted the stress at this location. It is possible that some error was introduced due to the difficult nature of getting such large blades to be in a neutral state while on the ground.

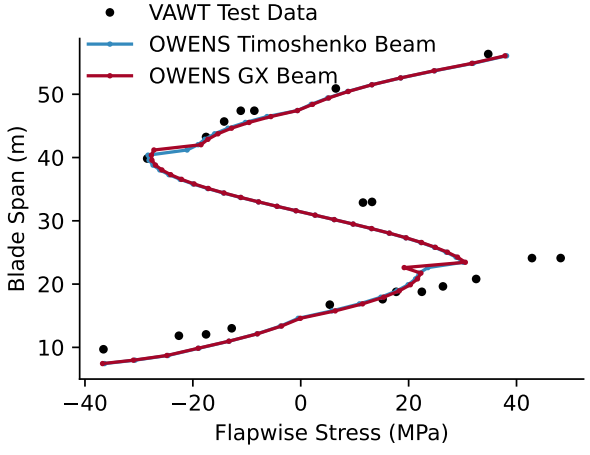

Figure 10. Gravity loads showing longitudinal stress along the blade.

https://doi.org/10.5194/wes-2022-91
Preprint. Discussion started: 10 October 2022

eawe european academy of wind energy
Open Access WIND ENERGY SCIENCE DISCUSSIONS

It should also be noted, that to model subsequent tests, we must follow the experimental procedure of zeroing out the gravity loads. Numerically, this means we need to run simulations with gravity and subtract the gravity-only loads. This is necessary to achieve the correct deformed blade shape under centrifugal loads and gravity since the centrifugal stress is very sensitive to the final deformed blade shape.

3.2.3 Still Air Centrifugal Loads

With the gravity loads known, we can run the still air centrifugal load cases. This is simply done by running a simulation with zero windspeed, but with the two-way aerodynamic model active to capture the drag forces on the blades. Figure 11a shows the resulting centrifugal stresses at 28 RPM and Fig. 11b at 40 RPM. Both cases show excellent agreement across the blade span.

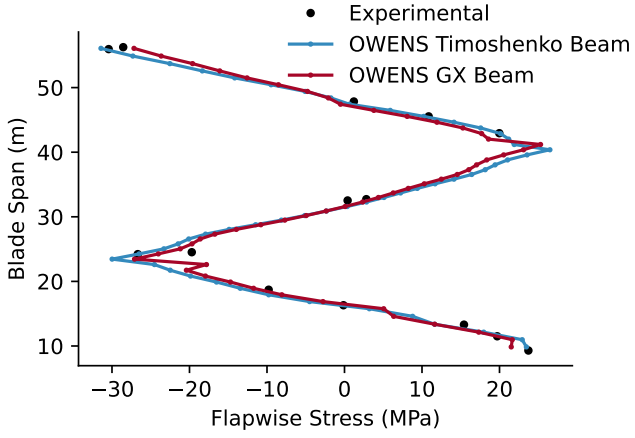

(a) 28 RPM forced spinning (calm wind) centrifugal stresses.

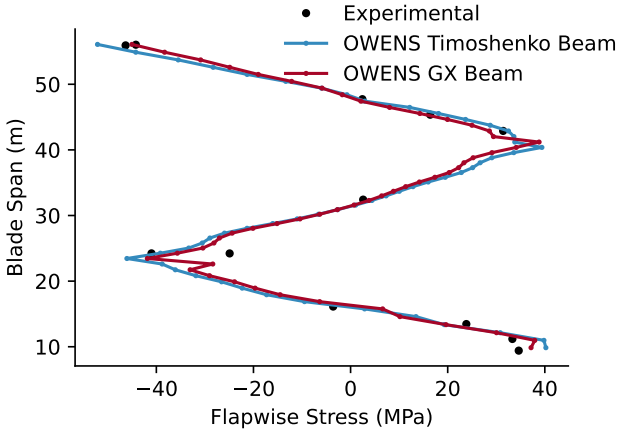

(b) 40 RPM forced spinning (calm wind) centrifugal stresses.

Figure 11. Centrifugal blade loads comparison.

3.2.4 Blade Shape and Centrifugal Stress Sensitivity

It should be noted that there is a very high sensitivity to the blade shape and centrifugal stress. When we compared the original drawings to digitized photographs of the 34m blade shape, we found as much as a 2.13% difference in blade shape (relative to the turbine diameter). While this is relatively small and has a negligible effect on the gravity stress, it has a large effect on the centrifugal stresses.

https://doi.org/10.5194/wes-2022-91
Preprint. Discussion started: 10 October 2022

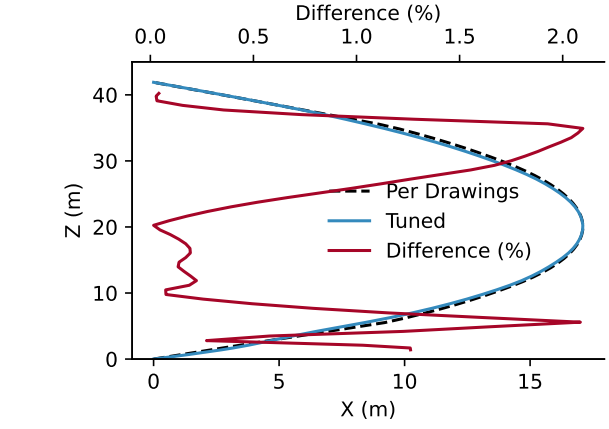

(a) SNL 34m blade shape, difference between shapes is less than 2.13% of the turbine diameter.

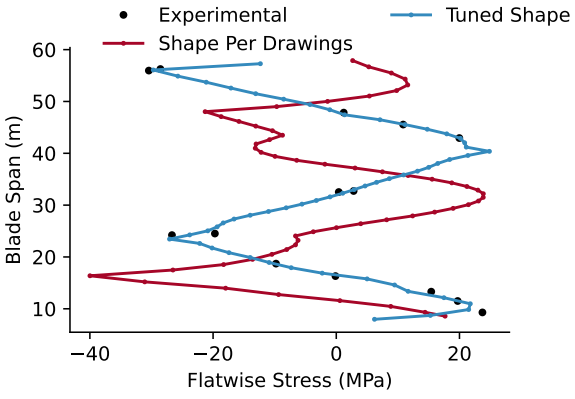

(b) 28 RPM centrifugal stress variation due to blade shape.

Figure 12. Sensitivity of blade shape on centrifugal loads.

Simply using the shape as given in the drawings, or the shape from legacy photos gives an overall trend of increasing and decreasing loads, similar to the experimental, but without general alignment and agreement. Due to this difference and sensitivity, we tuned the shape as shown in Fig. 12a within the known uncertainty to achieve a more realistic simulation, which is used in the analyses for this report. Figure 12 shows the relative difference between the shape per the drawings, and the tuned shape that was used.

3.3 SNL 34m Steady State Aeroelastic Performance Validation

The two generally used comparisons of overall turbine performance are the coefficient of performance, or efficiency, and torque. Verification and validation of the aerodynamics solver alone has been previously published (Moore and Ennis, 2022) so we primarily focus on the aeroelastic validation here. For a turbine operating at constant RPM, such as the Sandia 34m turbine operating at 34 RPM, high tip speed ratios occur at low wind speed and have low torque values, which can lead to a higher level of relative error in the power coefficient plot as seen in Fig. 13a. This is due to experimental uncertainty in the torque measurement at low values. Conversely, low tip speeds are in the stall operation region and the relative error is difficult to perceive in a power coefficient plot, but much easier to see in the torque plot as seen in Figure 13b. The maximum error for torque occurs in the low TSR, high wind speed regions, where the turbine is operating under significant variations in angle of attack and the dynamic stall models are active. This maximum error is approximately 15% on the torque predictions at low tip speed ratios.

https://doi.org/10.5194/wes-2022-91
Preprint. Discussion started: 10 October 2022

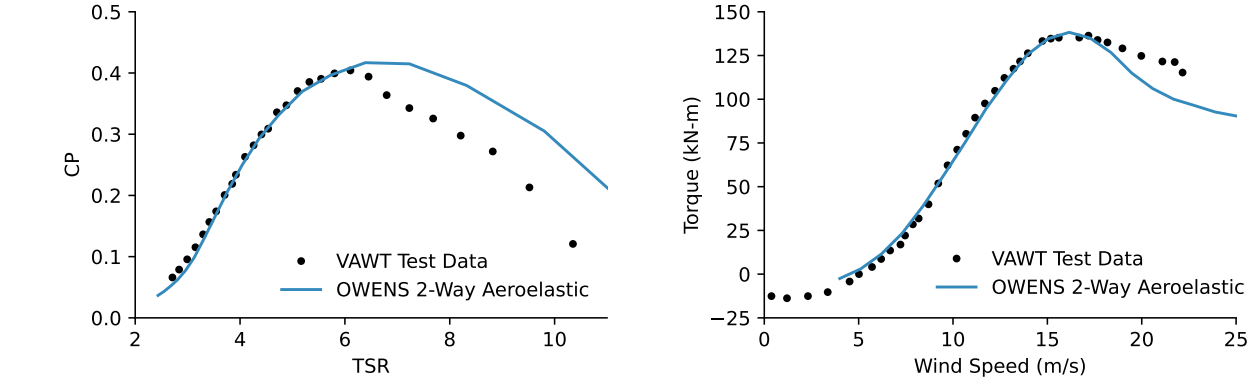

(a) Power Coefficient vs. Tip Speed Ratio

(b) Torque vs. Windspeed

Figure 13. Performance comparison for the Sandia 34 meter turbine operating at 34 RPM comparing experimental and 2-way aeroelastic coupling.

3.4 SNL 34m Dynamic Aeroelastic Validation

With the overall turbine loads validated, we now move to the dynamic aeroelastic validation. The Sandia 34 meter test campaign recorded and retained time-history data for startup, normal operation, normal stop, and emergency stop at the root sections of the blade. OWENS has the ability to use torque controls or directly specified RPM, with or without an active drivetrain spring-mass-damper model. The physical drivetrain system, as depicted in Fig. 14, included a purposefully compliant drivetrain via rubber isolators to attenuate the periodic blade-pass torque fluctuations by as much as 95%. The compliant drivetrain allowed the turbine to operate with an azimuthally varying RPM, which in turn changes the blade stresses. However, we have found that for this turbine, the change in blade stresses is small (less than 10%) and therefore either control method can be used as long as the compliant drivetrain model is active. For the normal operation case, we recreate the compliant drivetrain model and implement a simple PI controller to mimic the synchronous generator at normal operating conditions. For the other cases shown we simply use the specified RPM method as opposed to attempting to recreate the more complex startup and shutdown controllers.

https://doi.org/10.5194/wes-2022-91
Preprint. Discussion started: 10 October 2022

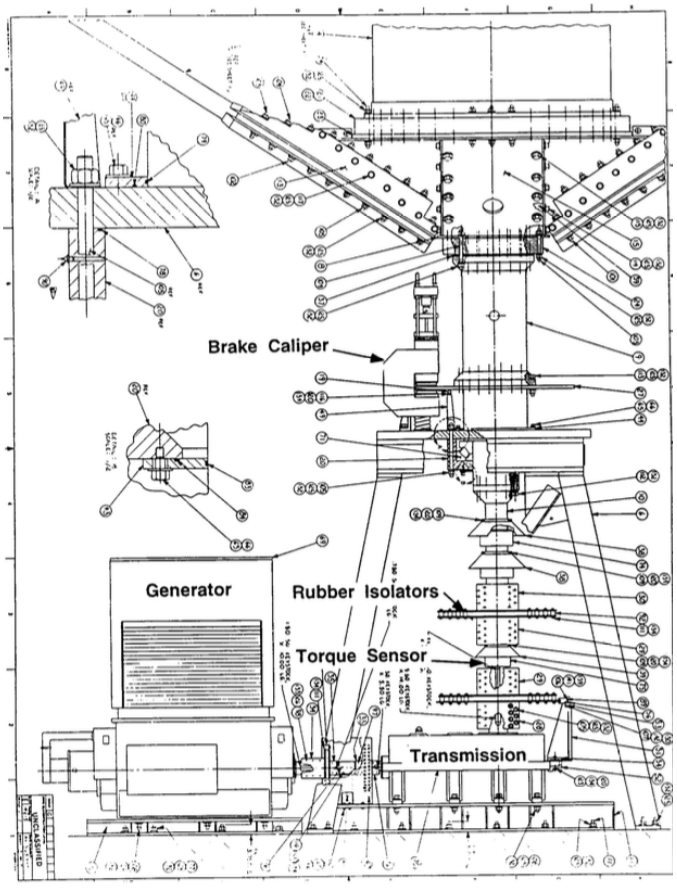

Figure 14. Sandia 34 meter turbine drivetrain.

3.4.1 Normal Operation

For normal operation, we recreated the drivetrain model and synchronous generator PI controller. Since the exact specifics of the design was not available at the time of writing, we used approximate values specified in Table 7. We first ran the simulation for 20 seconds with unchanging inputs to achieve steady state, and then supplied the measured windspeed uniformly across the rotor. Figure 16 shows a the normal operation torque. Despite the uncertainties in modeling and initial conditions, the macro torque variations are in line with the varying wind speed at the site. Some error is also introduced since the windspeed was measured at a single point adjacent to the turbine at the turbine equator as shown in Fig. 15.

https://doi.org/10.5194/wes-2022-91
Preprint. Discussion started: 10 October 2022

eawe european academy of wind energy
Open Access WIND ENERGY SCIENCE DISCUSSIONS

Table 7. Approximate drivetrain and driveshaft properties used for recreation of the 34m normal operation performance simulations.

Drivetrain Inertia	250.0 kg m2
Driveshaft Stiffness	10000 Nm/rad
Driveshaft Damping	1500 Nm/rad2
Torque Control Law	$Q_0 + K_p * RPM + K_i *$ Integral Error
K_p	10.63
K_i	5.26
Q_0	-320.15

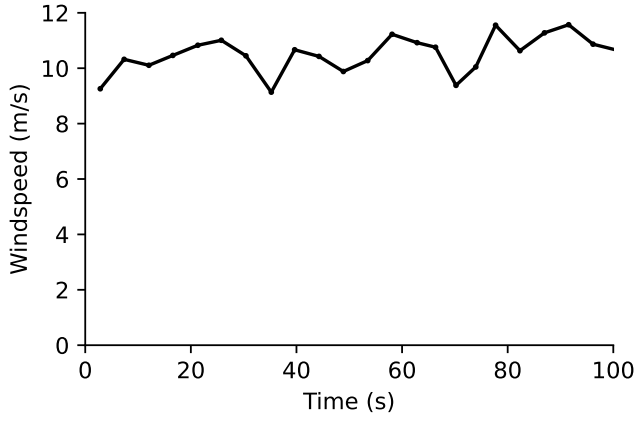

Figure 15. Recorded wind speed for the normal operation 34 RPM case.

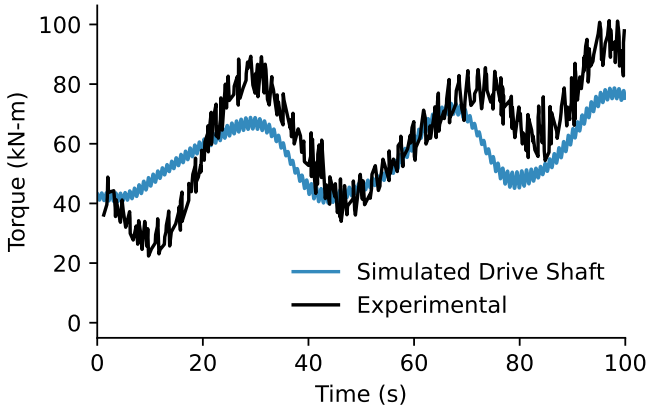

Figure 16. Turbine normal operation torque at 34 RPM.

Figures 17 and 18 show the flapwise and lead-lag simple stresses at the lower blade root. The strain gauges on the 34m turbine were installed in pairs, enabling pure bending moments to be measured, which is recreated here. The flapwise strain

https://doi.org/10.5194/wes-2022-91
Preprint. Discussion started: 10 October 2022

eawe european academy of wind energy
Open Access WIND ENERGY SCIENCE DISCUSSIONS

gauges were installed at the thickest portions of the symmetric airfoil, and the lead-lag strain gauges were installed effectively at the leading and trailing edges. The lead-lag stress was calculated based on the distance from the neutral axis to the trailing edge.

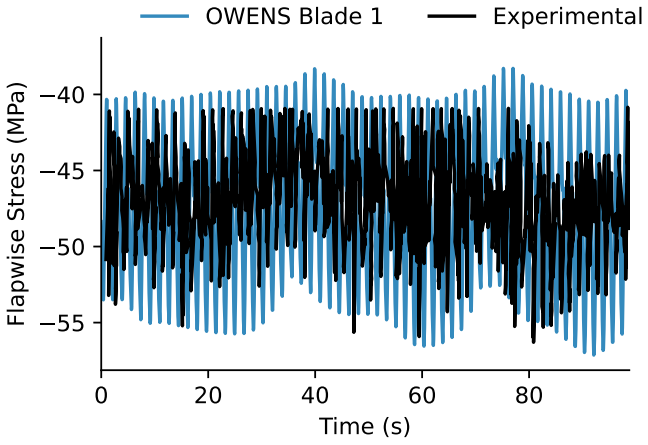

Figure 17. Turbine upper root normal operation flapwise stress at 34 RPM

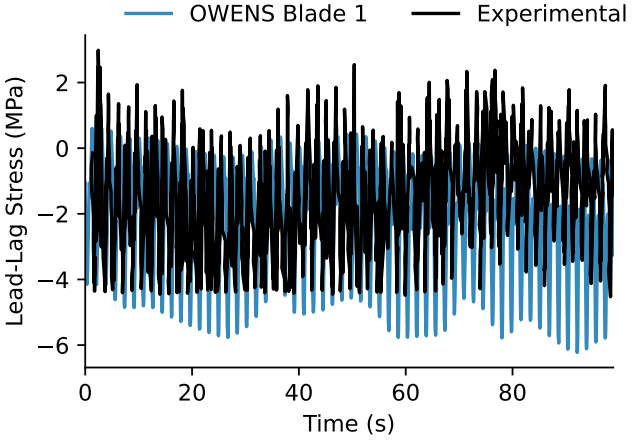

Figure 18. Turbine upper root normal operation lead-lag stress at 34 RPM

3.4.2 Emergency Stop

Emergency stop was modeled by running OWENS in the pre-specified RPM mode with the recorded RPM and windspeed as shown in Fig. 19. Figures 20 and 21 show the flapwise and lead-lag simple stresses. They show good agreement in the dynamics of stopping for both the mean and varying loads at the beginning, but deviate in the varying loads once the turbine RPM is significantly reduced. It is possible that a reduction in structural damping is needed depending on centrifugal loading.

https://doi.org/10.5194/wes-2022-91
Preprint. Discussion started: 10 October 2022

eawe european academy of wind energy
Open Access WIND ENERGY SCIENCE DISCUSSIONS

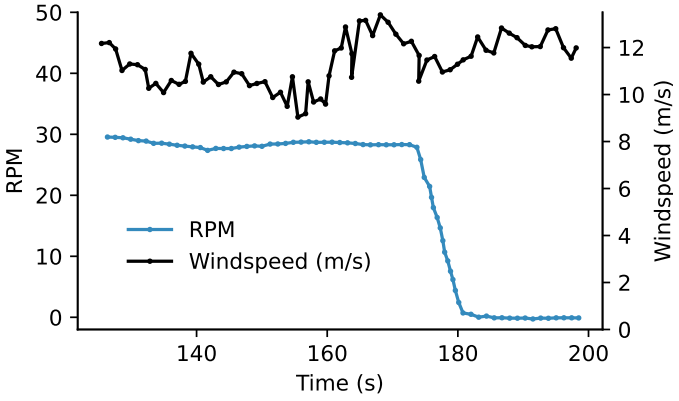

Figure 19. Turbine emergency stop used RPM and wind speed.

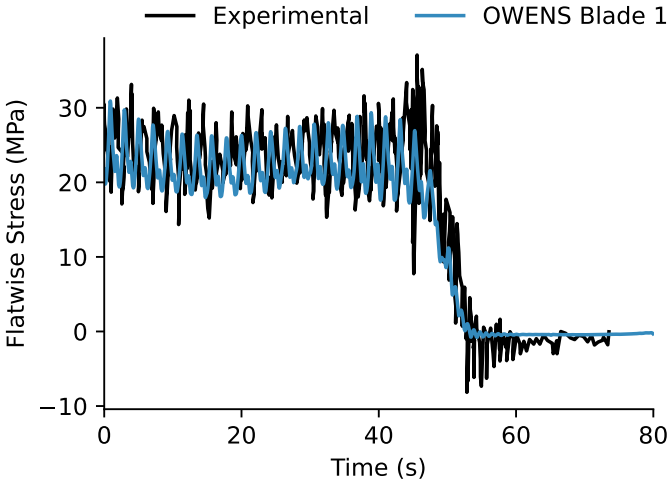

Figure 20. Turbine emergency stop lower root flapwise stress.

https://doi.org/10.5194/wes-2022-91
Preprint. Discussion started: 10 October 2022

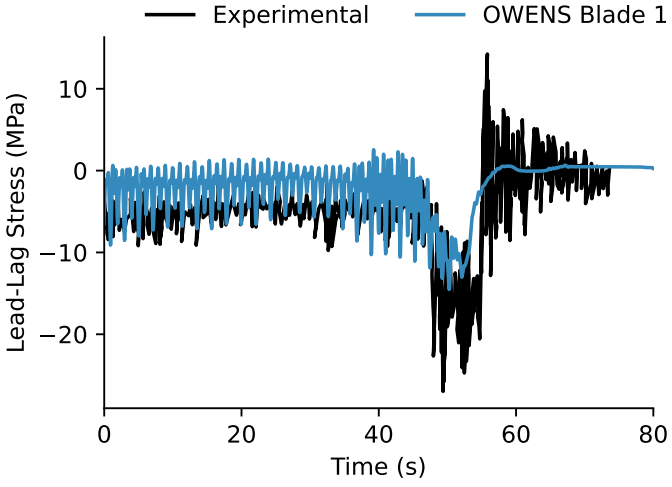

Figure 21. Turbine emergency stop lower root lead-lag stress.

3.4.3 Root Mean Variance

Though the 34m VAWT test campaign collected vast amounts of time data, the majority was summarized into what was termed the root mean variance, or RMV. This value is equivalent to the root mean square, but with the mean signal subtracted, and represents the principal oscillatory stress. The equation is summarized in Eq. (5).

$$\text{RMV} = \sqrt{mean\left(\left(\text{signal} - mean(\text{signal})\right)^2\right)} \tag{5}$$

In the original report (Ashwill, 1992), summary data is given for each active strain gauge location for both blades at varying wind speed, and at 28, 34, and 38 RPM. For the purposes of this paper, we show only a few key summary positions and discuss their impact. Namely, we show the upper and lower root, equator, and upper and lower quarter span locations. Figure 22 gives a visual location of the strain gauge A-Q locations.

https://doi.org/10.5194/wes-2022-91
Preprint. Discussion started: 10 October 2022

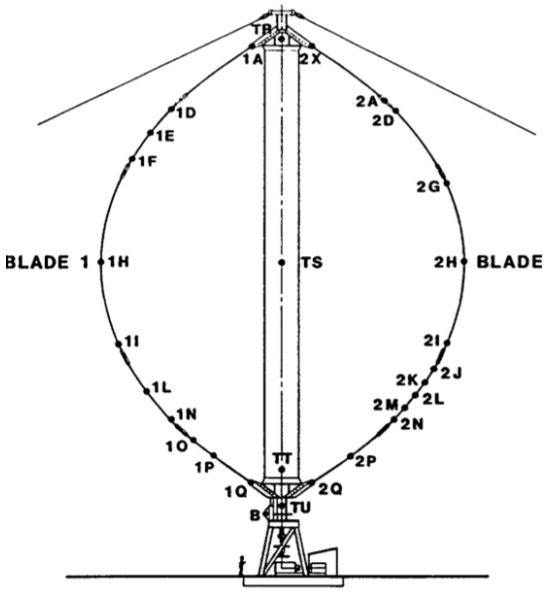

Figure 22. Sandia 34 meter turbine strain gauge locations.

To most accurately model the inflow conditions, we used TurbSim (Kelley and Jonkman, 2006) to generate a class C normal turbulence model (NTM) intensity flow field with a 0.05 second timestep for each of the wind speeds. This is in accordance with the closest known atmospheric conditions, which are at the Sandia SWiFT facility (Kelley and Ennis, 2016). While we use this turbulence model, there remains a significant amount of uncertainty in the actual turbulent inflow conditions during the experimental campaign, which should be taken into consideration when evaluating the differences between experimental and simulated results. In order to maintain steady state control of the turbine during the wide range of wind speeds, the generator control gains were scaled with the wind speed squared divided by 10.0 m/s squared (the original controller's design wind speed), in line with the standard wind turbine torque coefficient equation. The drivetrain model was unchanged. In the following plots, we divide both the experimental and simulated values by the simulated mean to give a relative comparison of the varying loads to the mean. The gauge identifier codes are interpreted as follows: the first character is the blade number, the second is the gauge location, the third is the type of strain measured (bending moment - M, axial - A), and the fourth is the direction (flapwise - F, lead-lag - L). For example, the 1AMF gauge is for blade 1, location A, moment, in the flapwise direction. The only deviation from this is the 1HF1 gauge, which was a backup gauge configured to measure flapwise moment at the H location.

Figures 23 to 27 show the upper root, upper quarter, equator, lower quarter, and lower root positions respectively. Overall there is good agreement in both flapwise and lead-lag loads, with the greatest deviation occurring for the equatorial flapwise loads in Fig. 25a and lower quarter lead-lag loads in Fig. 26b.

https://doi.org/10.5194/wes-2022-91
Preprint. Discussion started: 10 October 2022

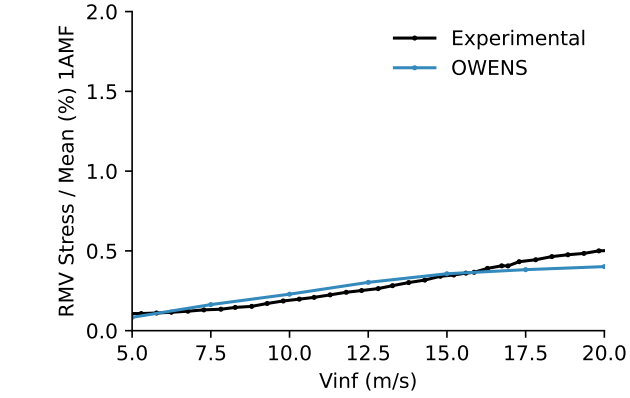

(a) Blade upper root flapwise RMV stress

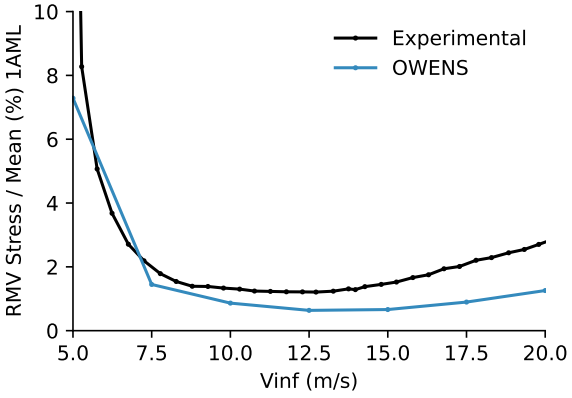

(b) Blade upper root lead-lag RMV stress

Figure 23. RMV stress percent of mean at the turbine upper root lag (1AMF) and flap (1AML) gauges at 34RPM with varying turbulent inflow velocity.

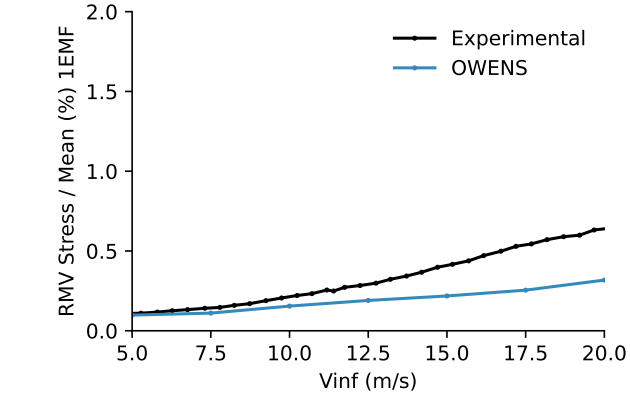

(a) Blade top quarter flapwise RMV stress

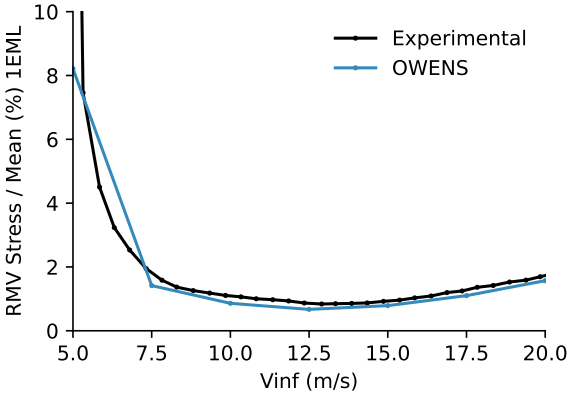

(b) Blade top quarter lead-lag RMV stress

Figure 24. RMV stress percent of mean at the turbine upper blade quarter lag (1EMF) and flap (1EML) gauges at 34RPM with varying turbulent inflow velocity.

https://doi.org/10.5194/wes-2022-91
Preprint. Discussion started: 10 October 2022

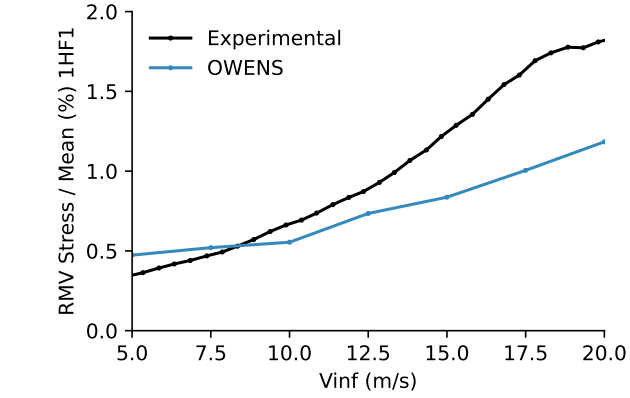

(a) Blade equator flapwise RMV stress

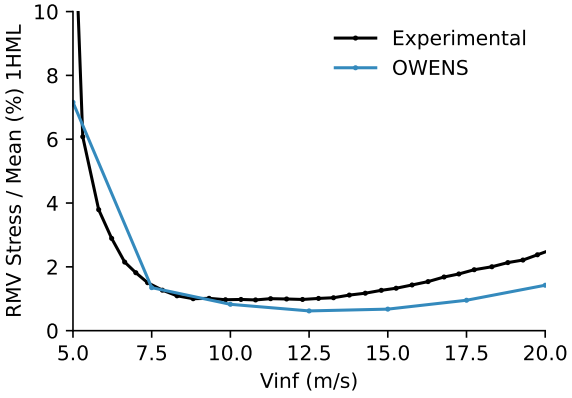

(b) Blade equator lead-lag RMV stress

Figure 25. RMV stress percent of mean at the turbine equator lag (1HF1) and flap (1HML) gauges at 34RPM with varying turbulent inflow velocity.

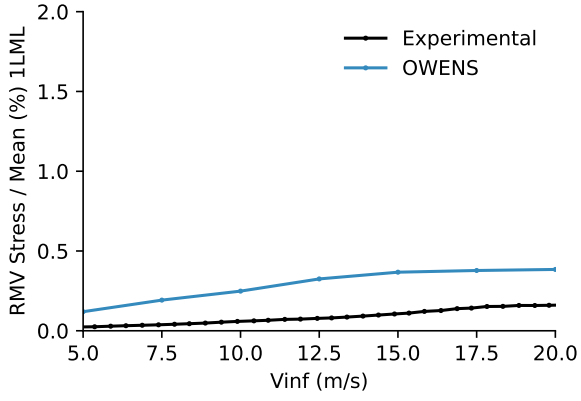

(a) Blade lower quarter flapwise RMV stress

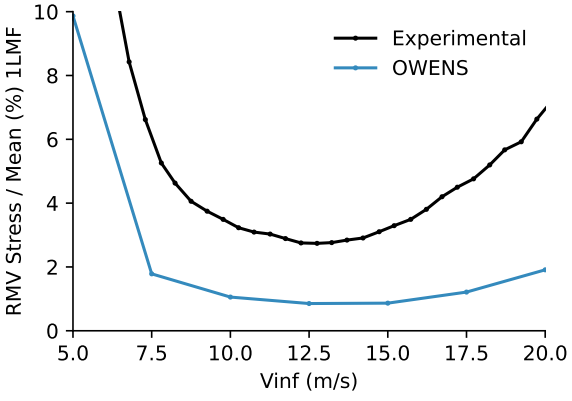

(b) Blade lower quarter lead-lag RMV stress

Figure 26. RMV stress percent of mean at the turbine lower quarter lag (1LMF) and flap (1LML) gauges at 34RPM with varying turbulent inflow velocity.

https://doi.org/10.5194/wes-2022-91
Preprint. Discussion started: 10 October 2022

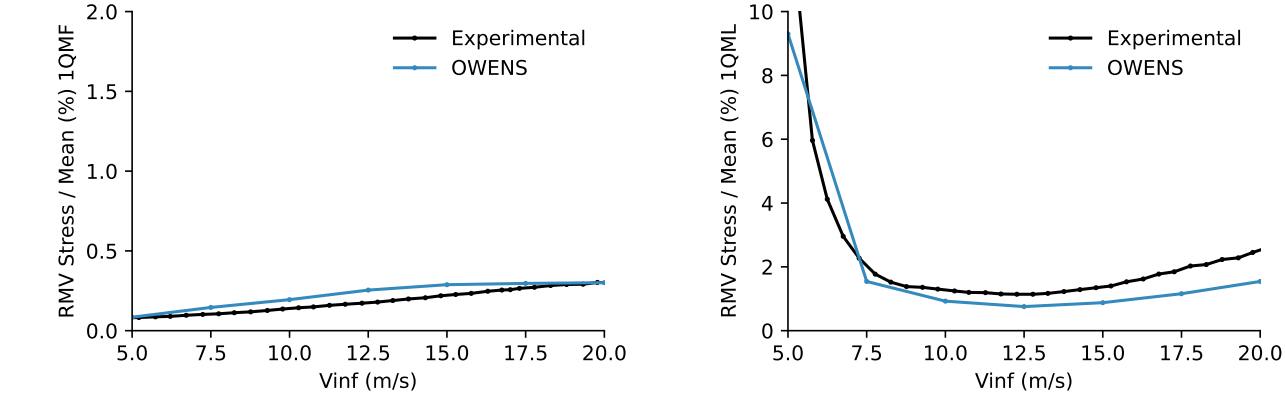

(a) Blade lower root flapwise RMV stress

(b) Blade lower root lead-lag RMV stress

Figure 27. RMV stress percent of mean at the turbine lower root lag (1QMF) and flap (1QML) gauges at 34RPM with varying turbulent inflow velocity.

4 Conclusions

A comprehensive validation hierarchy for aeroelastic predictions of vertical-axis wind turbines has been developed based on increasing complexity of analysis from simple structures with analytical solutions to an unsteady time domain simulation of a 500 kW VAWT. Predictions have been performed with the OWENS aero-hydro-servo-elastic design tool and compared to analytical solutions, to predictions using a geometrically exact beam theory model, and to experimental data from the legacy Sandia 34 meter VAWT testbed. Based on the set of validation cases presented, OWENS has been demonstrated to be able to predict the modal performance, including rotational effects, and the gravitational, centrifugal, and two-way aeroelastically-coupled dynamic turbine loads with turbulent inflow. The relative discrepancies between the experimental and predicted values have been reviewed and the analysis sensitivities discussed.

In a simple cantilever beam case, we validated performance with the analytical resonance predictions and linear tip deflections with differences less than 2%. We found excellent agreement with the higher-fidelity geometrically exact beam theory (GEBT) model for non-linear model operation with deflections up to 30% of the beam length where over-predictions were less than 3.3%. For modal, a maximum of 2.8% difference in the 6th mode of a rotating bent beam was observed, which could be attributed to the challenges associated with capturing torsional resonances with Timoshenko beams. In the nonlinear unsteady analysis, we found excellent agreement in capturing the damped natural frequency, but differences in the methods of structural damping between the the Timoshenko beam formulation and geometrically exact beam theory prevented a an exact comparison of the damped amplitudes.

When modeling the Sandia 34m VAWT, we found agreement in the resonance predictions, including rotational effects, through a Campbell diagram analysis. Static loading from gravitational and centrifugal effects were compared with a high level of accuracy, and we discussed the sensitivity of minor blade shape variations on the centrifugal stress for this type of

https://doi.org/10.5194/wes-2022-91
Preprint. Discussion started: 10 October 2022

eawe european academy of wind energy
Open Access WIND ENERGY SCIENCE DISCUSSIONS

turbine. We recreated an approximation of the turbulent inflow velocity, drivetrain, and generator and showed agreement with the attenuated torque, flapwise, and lead-lag bending data from legacy experiments for a range of operating conditions and locations along the blades.

In summary, we found a strong ability for OWENS to predict mean and varying loads for a large land-based VAWT despite uncertainties in the turbulent inflow and drivetrain models. Based on the performance of the OWENS code with the presented validation cases, there is high level of trust in two-way coupled aeroelastic predictions using the OWENS software to enable accurate design and certification of vertical-axis wind turbines.

Code availability. The OWENS code can be made available through the Sandia National Labs intellectual property department, ip.sandia.gov, SRC# 1617.

Author contributions. KRM performed the analyses, produced all figures, and drafted this article. BLE directed the work, advised and assisted in the model development and troubleshooting, and contributed significant edits to the article. All authors jointly finalized the article.

Competing interests. The authors declare that they have no conflict of interest.

Disclaimer. The views or opinions expressed herein do not necessarily state or reflect those of the United States Government, any agency thereof, or any of their contractors.

Acknowledgements. This work has been funded by the United States Department of Energy (DOE) Advanced Research Projects Agency – Energy (ARPA-e) under the ATLANTIS program.

https://doi.org/10.5194/wes-2022-91
Preprint. Discussion started: 10 October 2022

eawe european academy of wind energy
Open Access WIND ENERGY SCIENCE DISCUSSIONS

References

Alcoa: Design and fabrication of a low-cost Darrieus vertical-axis wind-turbine system, Phase II. Volume 2. Final technical report, Tech. rep., https://www.osti.gov/biblio/6321998, 1983.

Ashwill, T. D.: Measured data for the Sandia 34-meter vertical axis wind turbine, https://citeseerx.ist.psu.edu/viewdoc/download?doi=10.1.1.509.1110&rep=rep1&type=pdf, SAND-91-2228, 1992.

Bezanson, J., Edelman, A., Karpinski, S., and Shah, V. B.: Julia: A fresh approach to numerical computing, SIAM review, 59, 65–98, https://doi.org/10.1137/141000671, 2017.

Bir, G. S.: User's guide to PreComp (Pre-Processor for Computing Composite Blade Properties), National Renewable Energy Laboratory, https://search.library.wisc.edu/catalog/9910060034202121, 2006.

Blackwell, B. F., Sheldahl, R. E., and Feltz, L. V.: Wind tunnel performance data for the Darrieus wind turbine with NACA 0012 blades, https://doi.org/10.2172/7269797, 1976.

Darrieus, G. J. M.: Turbine Having its Rotating Shaft Transverse to the Flow of the Current, U.S. Patent, uS1835018A, 1926.

Hodges, D. H.: Nonlinear Composite Beam Theory, https://doi.org/https://doi.org/10.2514/4.866821, 2006.

Inman, D. J.: Engineering Vibrations, chap. 6, pp. 539, 608, Pearson, 4th edn., iSBN-13:9780132871723, 2014.

James M. Gere, B. J. G.: Mechanics of Materials, chap. 9, p. 805, Cengage Learning, iSBN-13: 978-81-315-2474-9, 2013.

Kelley, C. L. and Ennis, B. L.: SWiFT site atmospheric characterization, https://doi.org/10.2172/1237403, 2016.

Kelley, N. D. and Jonkman, B. J.: Overview of the TurbSim Stochastic Inflow Turbulence Simulator: Version 1.10, https://doi.org/10.2172/891590, 2006.

McDonnell, T. and Ning, A.: GXBeam: A Pure Julia Implementation of Geometrically Exact Beam Theory, Journal of Open Source Software, 7, 3997, https://doi.org/10.21105/joss.03997, 2022.

Meirovitch, L.: Computational Methods in Structural Dynamics, Stijhoff and Noordhoff International Publishers, Rockville, Maryland, 1980.

Moore, K. R. and Ennis, B. L.: Vertical-Axis Wind Turbine Steady and Unsteady Aerodynamics for Curved Deforming Blades, AIAA Journal, 60, 189–196, https://doi.org/10.2514/1.J060476, 2022.

NREL: OpenFAST. Open-source wind turbine simulation tool, available at http://github.com/OpenFAST/OpenFAST, 2022.

Oberkamph, W., Trucano, T., and Hirsch, C.: Verification, validation, and predictive capability in computational engineering and physics, Tech. Rep. SAND2003-3769, Sandia National Laboratories, 2003.

Owens, B. C.: Theoretical Developments and Practical Aspects of Dynamic Systems in Wind Energy Applications, Ph.D. thesis, Texas A&M, https://doi.org/https://hdl.handle.net/1969.1/151813, 2013.

Packman, P.: Aging Aircraft and Fatigue Failure, J. Air L. & Com., 54, 965, 1988.

Sheldahl, R. E., Klimas, P. C., and Feltz, L. V.: Aerodynamic Performance of a 5-Metre-Diameter Darrieus Turbine With Extruded Aluminum NACA-0015 Blades, Tech. Rep. SAND-80-0179, Sandia National Laboratories, 1980.

Sutherland, H. J.: Strain Gauge Validation Experiments for the Sandia 34-Meter VAWT Test Bed, Tech. Rep. SAND-88-1807, Sandia National Laboratories, 1988.

Wang, Q., Yu, W., and Sprague, M.: Geometric Nonlinear Analysis of Composite Beams using Wiener-Milenković Parameters, AIAA, https://doi.org/10.2514/6.2013-1697, 2013.

Worstell, M. H.: Aerodynamic Performance of the DOE/Sandia 17-m-Diameter Vertical-Axis Wind Turbine, Journal of Energy, 5, 39–42, https://doi.org/10.2514/3.62496, 1981.

https://doi.org/10.5194/wes-2022-91
Preprint. Discussion started: 10 October 2022

eawe european academy of wind energy
Open Access WIND ENERGY SCIENCE DISCUSSIONS

Yu, W. and Blair, M.: GEBT: A general-purpose nonlinear analysis tool for composite beams, Composite Structures, 94, 2677–2689, https://doi.org/https://doi.org/10.1016/j.compstruct.2012.04.007, https://github.com/byuflowlab/GXBeam.jl, 2012.